Comput. Methods Appl. Mech. Engrg. 245–246 (2012) 206–216

Contents lists available at SciVerse ScienceDirect

Comput. Methods Appl. Mech. Engrg.

journal homepage: www.elsevier.com/locate/cma

Modeling and simulation of electrification delivery in functionalized textiles in electromagnetic fields

T.I. Zohdi

Department of Mechanical Engineering, 6195 Etcheverry Hall, University of California, Berkeley, CA 94720-1740, USA

ARTICLE INFO

Article history:
Received 2 January 2012
Received in revised form 11 May 2012
Accepted 3 July 2012
Available online 20 July 2012

Keywords:
Textiles
Electromagnetism
Multiphysics
Dynamics

ABSTRACT

This work investigates the deformation of electrified textiles in the presence of an externally supplied magnetic field ($\boldsymbol{B}^{ext}$). The electrification is delivered by running current ($\boldsymbol{J}$) through the fibers from an external power source. Of primary interest is to ascertain the resulting electromagnetic forces imposed on the fabric, and the subsequent deformation, due to the terms $\boldsymbol{J}\times\boldsymbol{B}^{ext}$ and $\mathcal{P}\boldsymbol{E}$, where $\mathcal{P}$ is the charge density, $\boldsymbol{E}$ is the electric field and the current given by $\boldsymbol{J}=\sigma(\boldsymbol{E}+\boldsymbol{v}\times\boldsymbol{B}^{ext})$, where σ is the fabric conductivity, and $\boldsymbol{v}$ is the fabric velocity. As the fabric deforms, the current changes direction and magnitude, due to the fact that it flows through the fabric. The charge density is dictated by Gauss' law, $\nabla\cdot\boldsymbol{D}=\mathcal{P}$, where $\boldsymbol{D}=\epsilon\boldsymbol{E},\epsilon$ is the electrical permittivity and $\boldsymbol{D}$ is the electric field flux. In order to simulate such a system, one must solve a set of coupled equations governing the charge distribution, current flow and system dynamics. The deformation of the fabric, as well as the charge distribution and current flow, are dictated by solving the coupled system of differential equations for the motion of lumped masses, which are coupled through the fiber-segments under the action of electromagnetically-induced forces acting on a reduced order network model. In the work, reduced order models are developed for (a) Gauss' law ($\nabla\cdot\boldsymbol{D}=\mathcal{P}$), (b) the conservation of current/charge, $\nabla\cdot\boldsymbol{J}+\frac{\partial\mathcal{P}}{\partial t}=0$, and (c) the system dynamics, $\nabla\cdot\boldsymbol{T}+\boldsymbol{f}=\rho\frac{d\boldsymbol{v}}{dt}$, where $\boldsymbol{T}$ is the Cauchy stress and $\boldsymbol{f}$ represents the induced body forces, which are proportional to $\mathcal{P}\boldsymbol{E}+\boldsymbol{J}\times\boldsymbol{B}^{ext}$. A temporally-adaptive, recursive, staggering scheme is developed to solve this strongly coupled system of equations. We also consider the effects of progressive fiber damage/rupture during the deformation process, which leads to changes (reduction) in the electrical conductivity and permittivity throughout the network. Numerical examples are given, as well as extensions to thermal effects, which are induced by the current-induced Joule-heating.

1. Introduction

This work studies the deformation of electromagnetically-sensitive fabric (Figs. 1 and 2), induced by external mechanical, electric and magnetic fields. There are many applications for such materials, for example electromagnetic actuators, microelectromechanical systems (MEMS) and recently proposed electromagnetic ballistic fabric shields [58,61], whereby the Lorentz force is harnessed to enhance material resistance capabilities beyond purely mechanical effects, to help impede a high-velocity incoming projectile. In this analysis, we assume that the fabric can carry a charge. One way of achieving this is by adding, during fabrication, highly-conductive fine-scale particles to the usual polymer material that comprises most structural fabric. Alternatively, one can introduce conductive material via particle spray processing techniques. There are a variety of industrial particle deposition techniques, and we refer the reader to the surveys of the state of the art found in [28,29]. The "functionalization" or "tailoring" of materials by the addition of fine-scale material is a process that has a long history in engineering. The usual approach is to add particulates that possess a desired property to enhance a base (binder) material. There exist several methods to predict the resulting effective properties of materials with embedded particulates dating back to well over 100 years, for example to Maxwell [30,31] and Lord Rayleigh [40]. For a thorough analysis of many of such methods, see [44,23,21,33] for solid-mechanics oriented treatments and [15,16,56] for computational aspects. For a series of works on continuum modeling and finite-element simulation of the deformation of magnetoelastic functionalized membranes and films (for example mixtures of iron powder and polydimethylsiloxane), we refer the reader to recent studies by Barham et al. [4–8]. Applications for such materials are driven by the extensive sensor, actuator and MEMS industries. For specific applications, see [42,41,17,25,26,3,24,32].

The present study investigates the connection between the electromagnetic loading and fabric actuation, building on the recent analysis of Zohdi [58,61]. In those works, the charges were

E-mail address: zohdi@me.berkeley.edu

0045-7825/$ - see front matter © 2012 Elsevier B.V. All rights reserved.
http://dx.doi.org/10.1016/j.cma.2012.07.003

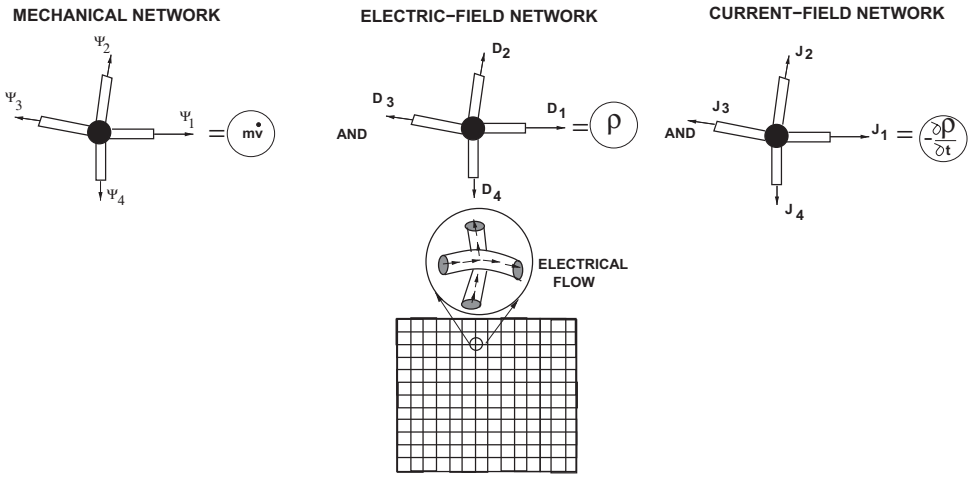

Fig. 1. A patch of fabric represented by network of woven-fabric by coupled fiber-segments. The fiber-segments are joined together by "pin-joint-like" connectors to form a network, whereby three sets of equations must be solved for the charge distribution, electric field and system dynamics.

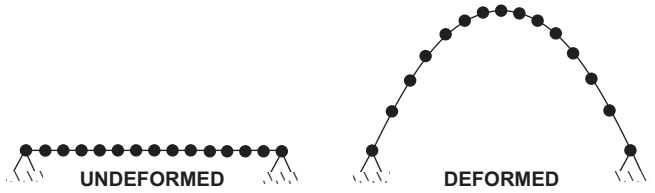

Fig. 2. A two-dimensional schematic of the deflection of the (lumped mass) fabric model, for a system that is clamped on both ends under (for example, unspecified, distributed) vertical loading. For details, on such models, see [47,54,58,48,52,38].

assumed to be electrostatic, i.e. intrinsically part of the fabric, in other words, the charges were considered to be *static within the fabric, i.e. not flowing*. For example, this type of "static" charge could be delivered in the form of an ion-implantation/bombardment/spray onto the fabric or, in some cases, one could consider materials that can be charged like a battery, provided that they have an inherent capacitance. However, in order to achieve much larger electric fields, a more robust, powerful and practical approach, is to run *live current* through the fabric system. This introduces a level of multifield complexity, both in terms of the modeling and simulation. *This is the focus of the analysis in this paper.*

The present work investigates the deformation of electrified textiles in the presence of an externally supplied magnetic field ($\boldsymbol{B}^{ext}$). The electrification is delivered by running current ($\boldsymbol{J}$) through the fibers from an external power source. Of primary interest is to ascertain the resulting electromagnetic forces imposed on the fabric, and the subsequent deformation, due to the terms $\boldsymbol{J}\times\boldsymbol{B}^{ext}$ and $\mathcal{P}\boldsymbol{E}$, where $\mathcal{P}$ is the charge density, $\boldsymbol{E}$ is the electric field and the current given by $\boldsymbol{J}=\sigma(\boldsymbol{E}+\boldsymbol{v}\times\boldsymbol{B}^{ext})$, where σ is the fabric conductivity, and $\boldsymbol{v}$ is the fabric velocity. As the fabric deforms, the current changes direction and magnitude, due to the fact that it flows through the fabric. The charge density is dictated by Gauss' law, $\nabla\cdot\boldsymbol{D}=\mathcal{P}$, where $\boldsymbol{D}=\epsilon\boldsymbol{E}$, ϵ is the electrical permittivity and $\boldsymbol{D}$ is the electric field flux. In order to simulate such a system, one must solve a set of coupled equations governing the charge distribution, current flow and system dynamics. The deformation of the fabric, as well as the charge distribution and current flow, are dictated by solving the coupled system of differential equations for the motion of lumped masses, which are coupled through the fiber-segments under the action of electromagnetically-induced forces acting on a reduced order network model.

Without any simplifications, such a system must be treated by direct continuum simulation of a fully coupled set of equations comprised of Maxwell's equations and the balance of momentum, which inevitably leads to non-trivial issues in numerical discretization and high-performance (large-scale) computing. Furthermore, depending on the type and level of actuation needed, the level of electromagnetism may induce thermal effects via Joule heating. A detailed account of full-blown continuum-based computational methods to simulate these effects can be found in [59] which employed the Finite Difference Time Domain Method (FDTD) and is beyond the scope of the current paper.[1] The development of reduced-order models that attempt to capture the essential features of such an electromagnetic delivery system, without resorting to full-scale, continuum, Maxwell-type, computations, is the subject of the present work. Specifically, reduced order models are developed for (a) Gauss' law ($\nabla\cdot\boldsymbol{D}=\mathcal{P}$), (b) the conservation of current/charge, $\nabla\cdot\boldsymbol{J}+\frac{\partial\mathcal{P}}{\partial t}=0$, and (c) the system dynamics, $\nabla\cdot\boldsymbol{T}+\boldsymbol{f}=\rho\frac{d\boldsymbol{v}}{dt}$, where $\boldsymbol{T}$ is the Cauchy stress and $\boldsymbol{f}$ represents the induced body forces, which are proportional to $\mathcal{P}\boldsymbol{E}+\boldsymbol{J}\times\boldsymbol{B}^{ext}$. A temporally-adaptive, recursive, staggering scheme is developed to solve this strongly coupled system of equations.

2. Fabric dynamics

The dynamics of the lumped charged-masses are given by

$$m_i\ddot{\boldsymbol{r}}_i=\underbrace{\boldsymbol{\Psi}_i^{tot}}_{\text{total}}=\underbrace{\boldsymbol{\Psi}_i^{em}}_{\text{electromagnetic forces}}+\underbrace{\sum_{I=1}^{4}\boldsymbol{\Psi}_{I_i}^{fiber}}_{\text{surrounding fiber}},\tag{2.1}$$

where $i=1,2,\ldots,N$, where N is the number of lumped charged-masses, $\boldsymbol{\Psi}_i^{em}$ represents the electromagnetic contribution, $\boldsymbol{\Psi}_{I_i}^{fiber}$ represents the contributions of the four fibers intersecting at charged-mass i (Fig. 1) and m_i is the mass of a single lumped charged-mass (the total fabric mass divided by the total number of charged-masses). The forces from the Ith surrounding fiber-segment (there are four of them for the type of rectangular weaving pattern considered) acting on the ith lumped charged-mass is $\boldsymbol{\Psi}_{I_i}^{fiber}$. Clearly, $\boldsymbol{\Psi}_{I_i}^{fiber}$ is a function of the charged-mass positions ($\boldsymbol{r}_i$), which are all coupled together, leading to a system of equations. In order to solve the resulting coupled system, we develop an iterative solution scheme later in the presentation.

[1] The primary alternative to FDTD is the Finite Element Method for electromagnetics. In particular, see [13,14] for the state of the art in adaptive Finite Element Methods for electromagnetics.

3. Fiber-segment network representation for mechanical forces

For the mechanical portion of the modeling of the fabric, we assume that: (1) the fiber-segments are quite thin, experiencing a uniaxial-stress condition, whereby the forces only act along the length of the fiber-segments, (2) the fiber-segments remain straight, undergoing a homogeneous (axial) stress state, (3) the compressive response of a fiber-segment is insignificant (relative to tensile states) and (4) fiber-segment buckling phenomena is ignored. We write one-dimensional constitutive laws in terms of the Piola–Kirchhoff stresses (mimicking 3-D approaches), defined by

$$P = \frac{\text{force on referential area}}{\text{referential area}} \tag{3.1}$$

and then transform the result to the second Piola–Kirchhoff stress via $P = US$, where $U = \frac{L}{L_o}$ is the stretch ratio, L is the deformed length of the fiber-segment, L_o is its original length and where we note that for a relaxed model, when $U \leqslant 1$ (compression), we enforce $P = 0$. A standard constitutive relation $S = \mathcal{F}(U)$ is then employed, with the primary objective being to extract the force carried in the fiber-segment (Ψ^{fiber}), which is needed later for the dynamics of the lumped charged-masses. Specifically,

$$P = \frac{\psi^{fiber}}{A_o} \Rightarrow \psi^{fiber} = USA_o = \frac{L}{L_o} SA_o. \tag{3.2}$$

We shall adopt a simple one-dimensional model for the stored energy, $W = \frac{1}{2}\mathbb{E}\mathcal{E}^2$, where $\mathbb{E}$ is Young's modulus and $\mathcal{E} \overset{\text{def}}{=} \frac{1}{2}(U^2 - 1)$ is the Green–Lagrange strain, with the second Piola–Kirchhoff stress given by $\frac{\partial W}{\partial \mathcal{E}} = S = \mathbb{E}\mathcal{E}$. Thus, for the fiber-segment,

$$P = \frac{\psi^{fiber}}{A_o} \Rightarrow \psi^{fiber} = USA_o = \frac{L}{L_o} SA_o = \frac{L}{2L_o}\mathbb{E}\left(\left(\frac{L}{L_o}\right)^2 - 1\right)A_o. \tag{3.3}$$

Remark 1. As a result of the previous analysis, $\Psi^{fiber}_{I_i} = U_I S_i A_o \boldsymbol{a}_{I_i}$ (A_o is the undeformed cross-sectional area of the fiber), where the unit axial fiber direction is given by $\boldsymbol{a}_{I_i} = \frac{\boldsymbol{r}^+_I - \boldsymbol{r}^-_I}{\|\boldsymbol{r}^+_I - \boldsymbol{r}^-_I\|}$, where $\boldsymbol{r}^+_I$ denotes the position vector of the endpoint connected to the lumped charged-mass and $\boldsymbol{r}^-_I$ denotes the endpoint that is connected to it neighboring charged-mass (Fig. 1).[2]

Remark 2. Assumption (3) the previous section is the adoption of a relaxed-type model, *whereby a zero stress state is enforced for a compressive state.* Relaxed models have a long history, and we refer the reader to works dating back to [36,9,34,10,35,11,12,43,18–20,1,2]. Relaxed formulations have served as a foundation for computational models describing rupture of ballistic fabric shielding in [47,54,58,48,52,38] and are the basis for the present approach.

Remark 3. Consistent with the assumed one-dimensional deformation of the fiber-segments, we have the following relations, between the deformed and undeformed states for the fiber-segment length ($U_I(t) = \frac{L_I(t)}{L_I(t=0)}$), cross-sectional area and volume:

$$\frac{V_I(t)}{V_I(t=0)} = \frac{A_I(t)L_I(t)}{A_I(t=0)L_I(t=0)} = U_I(t), \tag{3.4}$$

which renders $V_I(t) = V_I(t=0)U(t)$ and $A_I(t) = A_I(t=0)$ (the cross-sectional area remains constant). For other alternative possibilities for one-dimensional reduced-order model behavior see [48].

Remark 4. Further comments on the specific material development related to the computational model in this paper are included in Appendix A.

4. Modeling of current flow

4.1. Network model simplification

To describe the electromagnetic behavior of the network model, recall Gauss' law in integral form (posed over an arbitrary domain ω)

$$\int_{\partial\omega} \boldsymbol{D}\cdot\boldsymbol{n}\,dA = \int_{\omega} \mathcal{P}dV, \tag{4.1}$$

where $\boldsymbol{D}$ is the electrical field flux, $\mathcal{P}$ is the dynamic charge per unit volume. Similarly, for the conservation of charge in integral form

$$\int_{\partial\omega} \boldsymbol{J}\cdot\boldsymbol{n}dA + \int_{\omega} \frac{\partial \mathcal{P}}{\partial t} dV = 0, \tag{4.2}$$

where $\boldsymbol{J}$ is the current field. During the electromagnetic modeling, we assume that the electromagnetic fields have evolved to steady state on time-scales that are much shorter than the dynamics of the fabric. Therefore, $\frac{\partial \mathcal{P}}{\partial t} = 0$ is assumed throughout the remainder of this work, thus

$$\int_{\partial\omega} \boldsymbol{J}\cdot\boldsymbol{n}dA = 0. \tag{4.3}$$

Some further comments on this assumption appear in Appendix B. For a reduced-order network model, we re-express Eqs. (4.1) and (4.3) in terms of one-dimensional electrical flow (through the fiber-segments), characterized by fluxes in and out of nodes. Accordingly, Eq. (4.1) can be expressed as

$$\sum_I \boldsymbol{D}_{I_i}\cdot\boldsymbol{n}_i A_i = \mathcal{P}_i V_i \tag{4.4}$$

and Eq. (4.3) as

$$\sum_I \boldsymbol{J}_{I_i}\cdot\boldsymbol{n}_i A_i = 0, \tag{4.5}$$

where V_i is the volume associated with the node (half of each of the surrounding segments), and A_i is the cross-sectional area associated with each surrounding segment where the $\mathcal{P}_i$ are the lumped values from the surrounding fiber-segments, and the $\boldsymbol{D}_{I_i}$ is the electrical field flux in segment I associated with node i, with the following constitutive law

$$\boldsymbol{D}_{I_i} = \epsilon_{I_i}\boldsymbol{E}_{I_i}, \tag{4.6}$$

where $\boldsymbol{E}_{I_i}$ is the electrical field in segment I associated with node i, ϵ_{I_i} is the electrical permittivity, and the current is

$$\boldsymbol{J}_{I_i} = \sigma_{I_i}\left(\boldsymbol{E}_{I_i} + \boldsymbol{v}_{I_i}\times\boldsymbol{B}^{ext}_{I_i}\right), \tag{4.7}$$

where, for segment I associated with node i, σ_{I_i} is the electrical conductivity, $\boldsymbol{v}_{I,i}$ is the velocity, $\boldsymbol{B}^{ext}_{I_i}$ externally controlled magnetic field. We assume that each segment has a one-dimensional $\boldsymbol{E}-\boldsymbol{D}-\boldsymbol{J}$ field along its axis, for example, $\boldsymbol{E}_I = E\boldsymbol{t}_I$, $\boldsymbol{D}_I = D\boldsymbol{t}_I$ and $\boldsymbol{J}_I = J\boldsymbol{t}_I$, where $\boldsymbol{t}_I$ is the tangent to the segment, which will change due to the deformation of the fabric.[3] Furthermore, on the segment level, we assume that the field quantities are uniform in magnitude in a segment, although they may change value from segment to segment. Since $\boldsymbol{B}^{ext}$ is multidimensional and is externally controlled, it has components that are not along the axis of the fiber-segments. Furthermore, the segment velocity has components that are not

[2] $\|\cdot\|$ indicates the Euclidean norm in R^3.

[3] Since the segments are assumed to be straight, $\boldsymbol{t}_I$ is along the Ith segment.

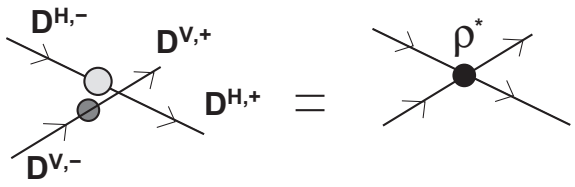

Fig. 3. Summing the horizontal and vertical flux contributions intersecting at a node and overlaying to obtain nodal quantities.

along the axis of the fiber-segments. However, *the (product) quantity,* $bf\, v_{I_i} \times \boldsymbol{B}^{ext}_{I_i}$, *in* $\boldsymbol{J}_{I_i} = \sigma_{I_i}\left(\boldsymbol{E}_{I_i} + \boldsymbol{v}_{I_i} \times \boldsymbol{B}^{ext}_{I_i}\right)$, *is projected onto the corresponding segment's tangent.* Explicitly (the term on the left should be interpreted as the term on the right),

$$\sigma_{I_i}(\boldsymbol{E}_{I_i} + \boldsymbol{v}_{I_i} \times \boldsymbol{B}^{ext}_{I_i}) \stackrel{\text{def}}{=} \sigma_{I_i}(\boldsymbol{E}_{I_i} \cdot \boldsymbol{t}_{I_i} + (\boldsymbol{v}_{I_i} \times \boldsymbol{B}^{ext}_{I_i}) \cdot \boldsymbol{t}_{I_i})\boldsymbol{t}_{I_i}. \tag{4.8}$$

Remark 1: The electromagnetic force induced on a segment I associated with node i is

$$\boldsymbol{F}_{I_i} = \left(\mathcal{P}_{I_i}\boldsymbol{E}_{I_i} + \boldsymbol{J}_{I_i} \times \boldsymbol{B}^{ext}_{I_i}\right)V_{I_i}. \tag{4.9}$$

The force experienced by the node i surrounded by the four segments is computed by taking the shares of the surrounding segments (half a segment from each side), $\frac{1}{2}\boldsymbol{F}_{I_i}$.

Remark 2: The charge in each segment is approximated as the average at the nodal endpoints $\mathcal{P}_{I_i} \approx \frac{\mathcal{P}^+_i + \mathcal{P}^-_i}{2}$. The velocity of each segment is approximated as the average at the nodal endpoints of the segment, $\boldsymbol{v}_{I_i} \approx \frac{\boldsymbol{v}^+_i + \boldsymbol{v}^-_i}{2}$.

4.2. Flux summation at nodes

We now provide details on the flux summation dictated by Eqs. 4.4 and 4.5. Referring to Fig. 3 (and Fig. 1), we assume that there is no charge transfer between the initially orthogonal networks of fiber-segments, although they are mechanically joined. This assumption allows the independent flux summation at a node in each fiber direction, which can then be added together to determine nodel quantities. In the *initially* horizontal (H) direction, we have (Gauss' Law)[4]

$$\mathcal{P}^H_i V^H_i = D^{H,+}_i A^{H,+}_i - D^{H,-}_i A^{H,-}_i, \tag{4.10}$$

where $D^{H,+}_i$ is the flux of the fiber-segment to the right of the node, $A^{H,+}_i$ is the cross-sectional area to the right of the node, $D^{H,-}_i$ is the flux of the fiber-segment to the left of the node, $A^{H,-}_i$ is the cross-sectional area to the left of the node and V^H_i is the average volume of the two segments. In the *initially* vertical (V) direction we have

$$\mathcal{P}^V_i V^V_i = D^{V,+}_i A^{H,+}_i - D^{V,-}_i A^{V,-}_i, \tag{4.11}$$

where $D^{V,+}_i$ is the flux of the fiber-segment above the node, $A^{V,+}_i$ is the cross-sectional area above the node, $D^{V,-}_i$ is the flux of the fiber-segment below the node, $A^{V,-}_i$ is the cross-sectional area below the node and V^V_i is the average volume of the two segments. Note that the volumes and areas change with the deformation of the body (as indicated previously), governed by the local one-dimensional deformation gradient. Adding the two previous equations together yields an expression for the conjoined system:

$$\mathcal{P}^*_i V^*_i \stackrel{\text{def}}{=} \mathcal{P}^H_i V^H_i + \mathcal{P}^V_i V^V_i = D^{H,+}_i A^{H,+}_i - D^{H,-}_i A^{H,-}_i + D^{V,+}_i A^{V,+}_i - D^{V,-}_i A^{V,-}_i, \tag{4.12}$$

where $V^*_i = V^H_i + V^V_i$, and $\mathcal{P}^*_i$ is the effective charge at a (cross-linked) node. The same holds for the current (from the conservation law), namely, in the initially horizontal direction, we have

$$J^{H,+}_i A^{H,+}_i - J^{H,-}_i A^{H,-}_i = 0 \tag{4.13}$$

and in the initially vertical direction

$$J^{V,+}_i A^{V,+}_i - J^{V,-}_i A^{V,-}_i = 0. \tag{4.14}$$

4.3. Solution process

The preceding relations lead to an implicit set of equations which are strongly coupled, as well as being coupled to the system dynamics via the term $\boldsymbol{v} \times \boldsymbol{B}^{ext}$ and Eq. (2.1). In order to deal with system, we employ a staggering scheme where, broadly speaking, the solution method sweeps through the system, *node by node, and segment by segment*, updating the variables as it progresses. Specifically (where K is an iteration counter and $\boldsymbol{B}^{ext}$ is considered fixed (externally controlled)),

1. Determine $\boldsymbol{D}^K_{I_i}$ from Eq. (4.6), segment by segment. Explicitly, for each segment I_i surrounding node i determine $\boldsymbol{D}^K_{I_i} = \epsilon_{I_i}\boldsymbol{E}^K_{I_i}$.
2. Determine $\boldsymbol{J}^K_{I_i}$ from Eq. (4.7), segment by segment. Explicitly, for each segment I_i surrounding node i, determine $\boldsymbol{J}^K_{I_i} = \sigma_{I_i}\left(\boldsymbol{E}^K_{I_i} + \boldsymbol{v}^K_{I_i} \times \boldsymbol{B}^{ext}_{I_i}\right)$. *Note that the presence of the fabric velocity* $\boldsymbol{v}$*, and the (moving) fiber-segment tangents* $\boldsymbol{t}$ *couples this equation to the dynamics of the system, represented by Eq. (2.1). The overall algorithm, coupling the two types of physics will be discussed momentarily.*
3. From Eq. (4.12), solve for $\mathcal{P}^{*,K+1}_i$, with the $\boldsymbol{J}^K_{I_i}$ and $\boldsymbol{E}^K_{I_i}$ fixed, where during the individual nodal i update, all other nodal and segmental values are fixed. Explicitly, for the nodes, one solves for the effective charge via

$$\mathcal{P}^{*,K+1}_i = \left(\frac{1}{V^*_i}\left(D^{H,+}_i A^{H,+}_i - D^{H,-}_i A^{H,-}_i + D^{V,+}_i A^{V,+}_i - D^{V,-}_i A^{V,-}_i\right)\right)^K \tag{4.15}$$

and for E_{I_i}, from Eq. (4.13), we have

$$\begin{aligned} J^{H,+}_i A^{H,+}_i - J^{H,-}_i A^{H,-}_i = 0 \Rightarrow & \underbrace{(\sigma(\boldsymbol{E} + \boldsymbol{v} \times \boldsymbol{B}))^{H,+}}_{J^{H^+}} A^{H,+} \\ & = \underbrace{(\sigma(\boldsymbol{E} + \boldsymbol{v} \times \boldsymbol{B}))^{H,-}}_{J^{H,-}} A^{H,-} \end{aligned} \tag{4.16}$$

and Eq. (4.14)

$$\begin{aligned} J^{V,+}_i A^{V,+}_i - J^{V,-}_i A^{V,-}_i = 0 \Rightarrow & \underbrace{(\sigma(\boldsymbol{E} + \boldsymbol{v} \times \boldsymbol{B}))^{V,+}}_{J^{V^+}} A^{V,+} \\ & = \underbrace{(\sigma(\boldsymbol{E} + \boldsymbol{v} \times \boldsymbol{B}))^{V,-}}_{J^{V,-}} A^{V,-}, \end{aligned} \tag{4.17}$$

which can be written

$$\boldsymbol{E}^{K+1,V,+} = \underbrace{\left[\frac{1}{\sigma^{V,+}A^{V,+}}(\sigma(\boldsymbol{E} + \boldsymbol{v} \times \boldsymbol{B}))^{V,-}A^{V,-} - (\boldsymbol{v} \times \boldsymbol{B})^{V,+}\right]^K}_{\text{evaluated at } K \text{ th iteration}}. \tag{4.18}$$

4. This process is repeated and updated for all of the nodes and segments.

[4] The nomenclature of "initially horizontal" and "initially vertical" is used since after the fabric deforms the fibers are neither horizontal nor vertical, nor mutually orthogonal.

5. The dynamics equation (Eq. (2.1)) is then solved for the motion of the nodes, *freezing the electromagnetic variables*, using the Lorentz force for each segment (see comments associated with Eq. (4.9)):

$$\boldsymbol{\Psi}_i^{em,K+1} = \sum_{l=1}^{4} \frac{1}{2} \boldsymbol{F}_{l_i}^{K+1}. \tag{4.19}$$

Afterwards, the current field is updated, segment by segment

$$\boldsymbol{J}_{l_i}^{K+1} = \sigma_{l_i} \left(\boldsymbol{E}_{l_i}^{K+1} + \boldsymbol{v}_{l_i}^{K+1} \times \boldsymbol{B}_{l_i}^{ext} \right). \tag{4.20}$$

and the entire procedure (all previous steps) is repeated.

For related, detailed, electrostatically charged-mass interaction formulations and simulation techniques, we refer the reader to [49–60].

5. Damage evolution in a fiber-segment network

Until this point, we have not included fiber damage in the formulation. Generally, the microstructure of the fabric fibers is composed of several microscale fibrils. For example, fabric materials such as Zylon, which is a polymeric material produced by the Toyobo Corporation [45], Kevlar and other aramid-based materials have a microstructure comprised of bundles of microscale "microfibrils" forming the fibers, which is then tightly woven into sheets. For Zylon, each fiber contains approximately 350 microfibrils, which are randomly misaligned within the fiber, leading to a gradual type of failure, since the microfibrils become stretched to different lengths (within the fiber), when the fiber is in tension. A simple approach [52] to describe failure of a fiber is to check whether a critical stretch (for a fiber-segment) has been attained or exceeded, $U(t) \geqslant U_{crit}$, and to track the progressive damage with a single damage (isotropic) variable, α, used in $S = \alpha \mathbb{E} \mathcal{E}$, where $0 \leqslant \alpha \leqslant 1$. The damage variable for each fiber-segment typically has an evolution law associated with it, which represents progressive stretch-induced damage.[5] Specifically, for a fiber that is undamaged, $\alpha = 1$, while for a fiber that is completely damaged, $\alpha = 0$. For illustration purposes, for example, we adopt the damage representation of [52]

$$\alpha_I(t) = min\left(\alpha_I(0 \leqslant t^* < t), e^{\left(-\lambda\left(\frac{U(t)-U_{crit}}{U_{crit}}\right)\right)} \right), \tag{5.1}$$

where $\alpha_I(U(t=0)) = 1, U(t)$ is the stretch of the fiber-segment I at time t, and where $0 \leqslant \lambda$ is a damage decay parameter. The above relation indicates that damage is irreversible, i.e. α_I is a monotonically decreasing function. As $\lambda \to \infty$, the type of failure tends towards sudden rupture, while as $\lambda \to 0$, then there is no damage generated. The progressive damage of fibers can be written for the material constants as, for the Young's modulus,

$$\mathbb{E}(t) = \alpha \mathbb{E}(t_o) \tag{5.2}$$

and for the conductivity

$$\sigma(t) = \alpha \sigma(t_o) \tag{5.3}$$

and for the permittivity

$$\epsilon(t) = (\epsilon(t_o) - \epsilon^*)\alpha + \epsilon^* \tag{5.4}$$

where ϵ^* is the free-space permittivity. Note that as $\alpha \to 0$, the physical trends are $\mathbb{E}(t) \to 0$, $\sigma(t) \to 0$ and $\epsilon(t) \to \epsilon^*$. The damage variable is relatively easy to track during the staggering scheme. For detailed analysis of damage in materials at the microscale, we refer the reader to [15,16].

[5] Multiscale and damage formulations for structural fibers have been explored in detail in [48,52,38,58].

6. Overall numerical solution scheme

In order describe the overall time-stepping scheme, we first start with the dynamics of a single (i)th lumped charged-mass (Eq. (2.1)).

6.1. Adaptive time-stepping scheme

Following Zohdi [49–58], employing a trapezoidal-like rule ($0 \leqslant \phi \leqslant 1$), we have

$$\frac{\boldsymbol{v}_i(t+\Delta t) - \boldsymbol{v}_i(t)}{\Delta t} = \dot{\boldsymbol{v}}_i(t + \phi \Delta t) \tag{6.1}$$

and

$$\begin{aligned} \boldsymbol{v}_i(t+\Delta t) &= \boldsymbol{v}_i(t) + \frac{1}{m_i} \int_t^{t+\Delta t} \boldsymbol{\Psi}_i^{tot} \, dt \\ &= \frac{\Delta t}{m_i} \left(\phi \boldsymbol{\Psi}_i^{tot}(t+\Delta t) + (1-\phi) \boldsymbol{\Psi}_i^{tot}(t) \right). \end{aligned} \tag{6.2}$$

The position can be computed via by applying the mid-point rule again, yielding

$$\begin{aligned} \boldsymbol{r}_i(t+\Delta t) = \boldsymbol{r}_i(t) + \boldsymbol{v}_i(t)\Delta t + \frac{\phi(\Delta t)^2}{m_i} \big(\phi \boldsymbol{\Psi}_i^{tot}(\boldsymbol{r}_i(t+\Delta t)) \\ + (1-\phi) \boldsymbol{\Psi}_i^{tot}(\boldsymbol{r}_i(t)) \big) + \hat{\mathcal{O}}(\Delta t)^2, \end{aligned} \tag{6.3}$$

where if $\phi = 1$, then Eq. (6.3) becomes the (implicit) Backward Euler scheme, which is very stable, dissipative and $\hat{\mathcal{O}}(\Delta t)^2 = \mathcal{O}(\Delta t)^2$ locally in time, if $\phi = 0$, then Eq. (6.3) becomes the (explicit) Forward Euler scheme, which is conditionally stable and $\hat{\mathcal{O}}(\Delta t)^2 = \mathcal{O}(\Delta t)^2$ locally in time and if $\phi = 0.5$, then Eq. (6.3) becomes the (implicit) Midpoint scheme, which is stable and $\hat{\mathcal{O}}(\Delta t)^2 = \mathcal{O}(\Delta t)^3$ locally in time.[6] Eq. (6.3) can be solved recursively by recasting the relation as

$$\boldsymbol{r}_i^{L+1,K} = \mathcal{G}(\boldsymbol{r}_i^{L+1,K-1}) + \mathcal{R}_i, \tag{6.4}$$

where $K = 1, 2, 3, \ldots$ is the index of iteration within time step $L+1$ and $\mathcal{R}_i$ is a remainder term that does not depend on the solution, i.e. $\mathcal{R}_i \neq \mathcal{R}_i(\boldsymbol{r}_1^{L+1}, \boldsymbol{r}_2^{L+1} \ldots \boldsymbol{r}_N^{L+1})$. The convergence of such a scheme is dependent on the behavior of $\mathcal{G}$. Namely, a sufficient condition for convergence is that $\mathcal{G}$ is a contraction mapping for all $\boldsymbol{r}_i^{L+1,K}, K = 1, 2, 3 \ldots$ In order to investigate this further, we define the iteration error as $\boldsymbol{\varpi}_i^{L+1,K} \stackrel{\text{def}}{=} \boldsymbol{r}_i^{L+1,K} - \boldsymbol{r}_i^{L+1}$. A necessary restriction for convergence is iterative self consistency, i.e. the "exact" (discretized) solution must be represented by the scheme

$$\mathcal{G}(\boldsymbol{r}_i^{L+1}) + \mathcal{R}_i = \boldsymbol{r}_i^{L+1}. \tag{6.5}$$

Enforcing this restriction, a sufficient condition for convergence is the existence of a contraction mapping

$$\| \underbrace{\boldsymbol{r}_i^{L+1,K} - \boldsymbol{r}_i^{L+1}}_{\boldsymbol{\varpi}_i^{L+1,K}} \| = \| \mathcal{G}(\boldsymbol{r}_i^{L+1,K-1}) - \mathcal{G}(\boldsymbol{r}_i^{L+1}) \| \leqslant \eta^{L+1,K} \| \boldsymbol{r}_i^{L+1,K-1} - \boldsymbol{r}_i^{L+1} \|, \tag{6.6}$$

where, if $0 \leqslant \eta^{L+1,K} < 1$ for each iteration K, then $\boldsymbol{\varpi}_i^{L+1,K} \to \boldsymbol{0}$ for any arbitrary starting value $\boldsymbol{r}_i^{L+1,K=0}$, as $K \to \infty$. This type of contraction condition is sufficient, but not necessary, for convergence. Explicitly, the recursion is

[6] In order to streamline the notation, we drop the cumbersome $\mathcal{O}(\Delta t)$-type terms.

$$\boldsymbol{r}_i^{L+1,K} = \underbrace{\boldsymbol{r}_i^L + \boldsymbol{v}_i^L \Delta t + \frac{\phi(\Delta t)^2}{m_i}\left((1-\phi)\boldsymbol{\Psi}_i^{tot,L}\right)}_{\mathcal{R}_i} + \underbrace{\frac{\phi(\Delta t)^2}{m_i}\left(\phi \boldsymbol{\Psi}_i^{tot,L+1,K-1}\right)}_{\mathcal{G}(\boldsymbol{r}_i^{L+1,K-1})}, \tag{6.7}$$

where

$$\boldsymbol{\Psi}_i^{tot,L} = \boldsymbol{\Psi}_i^{tot,L}(\boldsymbol{r}_1^L, \boldsymbol{r}_2^L \ldots \boldsymbol{r}_N^L) \tag{6.8}$$

and

$$\boldsymbol{\Psi}_i^{tot,L+1,K-1} = \boldsymbol{\Psi}_i^{tot,L+1,K-1}\left(\boldsymbol{r}_1^{L+1,K-1}, \boldsymbol{r}_2^{L+1,K-1} \ldots \boldsymbol{r}_N^{L+1,K-1}\right). \tag{6.9}$$

The overall objective is to simultaneously maximize the time-step sizes to decrease overall computing time, while obeying an error tolerance on the numerical solution's accuracy.[7] In order to achieve this goal, we follow an approach found in Zohdi [49–58], originally developed for continuum thermo-chemical multifield problems where (1) one approximates $\eta^{L+1,K} \approx S(\Delta t)^p$ (S is a constant) and (2) one assumes that the error within an iteration to behave according to $(S(\Delta t)^p)^K \varpi^{L+1,0} = \varpi^{L+1,K}$, $K = 1, 2, \ldots$, where $\varpi^{L+1,0}$ is the initial norm of the iterative error and S is intrinsic to the system.[8] The objective is to meet an error tolerance in exactly a preset number of iterations. To this end, one writes $(S(\Delta t_{\text{tol}})^p)^{K_d} \varpi^{L+1,0} = TOL$, where TOL is a tolerance and where K_d is the number of desired iterations.[9] If the error tolerance is not met in the desired number of iterations, the contraction constant $\eta^{L+1,K}$ is too large. Accordingly, one can solve for a new smaller step size, under the assumption that S is constant

$$\Delta t_{\text{tol}} = \Delta t \left(\frac{\left(\frac{TOL}{\varpi^{L+1,0}}\right)^{\frac{1}{pK_d}}}{\left(\frac{\varpi^{L+1,K}}{\varpi^{L+1,0}}\right)^{\frac{1}{pK}}} \right). \tag{6.10}$$

Remarks: Numerous parameter studies using Eq. (6.10) can be found in [49–58]. The assumption that S is constant is not crucial, since the time steps are to be recursively refined and unrefined throughout the simulation.

6.2. Algorithm

An implementation of the procedure is as follows:

(1) GLOBAL FIXED − POINT ITERATION : (INITIALLY SET i = 1 AND K = 0) :
(2) IF i > N THEN GO TO (4) (N = # OF CHARGED − MASSES)
(3) IF i ≤ N THEN :
  (a) COMPUTE ELECTROMAGNETIC FIELDS : $\mathcal{P}_i^{*,L+1,K}$, $\boldsymbol{J}_{I_i}^{L+1,K}$, AND $\boldsymbol{E}_{I_i}^{L+1,K}$
  (b) COMPUTE CHARGED − MASS VELOCITY AND POSITION : $\boldsymbol{v}_i^{L+1,K}$, $\boldsymbol{r}_i^{L+1,K}$
  (c) COMPUTE NETWORK DAMAGE : $\alpha_I^{L+1,K}$
  (d) GO TO (2) AND NEXT MASS (i = i + 1)
(4) ERROR MEASURE :
  (a) $\varpi_K \overset{\text{def}}{=} \dfrac{\sum_{i=1}^N ||\boldsymbol{r}_i^{L+1,K} - \boldsymbol{r}_i^{L+1,K-1}||}{\sum_{i=1}^N ||\boldsymbol{r}_i^{L+1,K} - \boldsymbol{r}_i^L||}$ (normalized)
  (b) $Z_K \overset{\text{def}}{=} \dfrac{\varpi_K}{TOL_r}$
  (c) $\Phi_K \overset{\text{def}}{=} \left(\dfrac{\left(\frac{TOL}{\varpi_0}\right)^{\frac{1}{pK_d}}}{\left(\frac{\varpi_K}{\varpi_0}\right)^{\frac{1}{pK}}} \right)$
(5) IF TOLERANCE MET ($Z_K \leq 1$) AND $K < K_d$ THEN :
  (a) INCREMENT TIME : $t = t + \Delta t$
  (b) CONSTRUCT NEW TIME STEP : $(\Delta t)^{new} = \Phi_K (\Delta t)^{old}$,
  (c) SELECT MINIMUM : $\Delta t = MIN(\Delta t^{lim}, (\Delta t)^{new})$ AND GO TO (1)
(6) IF TOLERANCE NOT MET ($Z_K > 1$) AND $K < K_d$ THEN :
  (a) UPDATE ITERATION K = K + 1
  (b) RESET PARTICLE COUNTER i = 1
  (c) GO TO (2)
(7) IF TOLERANCE NOT MET ($Z_K > 1$) AND $K = K_d$ THEN :
  (a) CONSTRUCT NEW TIME STEP : $\Delta t = \Phi_K \Delta t$
  (b) RESTART AT TIME = t AND GO TO (1)

(6.11)

Remark 1: The expression in Eq. (6.10) can also be used for time step enlargement (to reduce computational effort) if convergence is met in less than K_d iterations.

Remark 2: External damping (for example from the environment) can easily be incorporated by adding $c_i \dot{\boldsymbol{r}}_i$ in the equations of motion:

$$m_i \ddot{\boldsymbol{r}}_i = \underbrace{\boldsymbol{\Psi}_i^{tot}}_{total} = \underbrace{\boldsymbol{\Psi}_i^{em}}_{\text{electromagnetic forces}} + \underbrace{\sum_{I=1}^4 \boldsymbol{\Psi}_{I_i}^{fiber}}_{\text{surrounding fiber}} - \underbrace{c_i \dot{\boldsymbol{r}}_i}_{\text{damping}} \tag{6.12}$$

7. Numerical examples: model problems with bidirectional current

As a model problem, we consider the presence of:

- a static magnetic field, $\boldsymbol{B}^{ext} = B_1^{ext}\boldsymbol{e}_1 + B_2^{ext}\boldsymbol{e}_2$ and
- an electric field pumped (controlled) in the $\boldsymbol{e}_1$ and $\boldsymbol{e}_2$ directions on the boundary (Fig. 4).

[7] According to Eq. (6.7), convergence is scaled by $\eta \propto \frac{(\Delta t)^2}{m_i}$, and that the contraction constant of $\mathcal{G}(\boldsymbol{\Psi})$ is (1) directly dependent on the magnitude of the interaction forces, (2) inversely proportional to the lumped masses m_i and (3) directly proportional to Δt. Thus, if convergence is slow within a time step, the time step size, which is adjustable, can be reduced by an appropriate amount to increase the rate of convergence.

[8] For the class of problems under consideration, due to the quadratic dependency on Δt, $p \approx 2$.

[9] Typically, K_d is chosen to be between five to ten iterations.

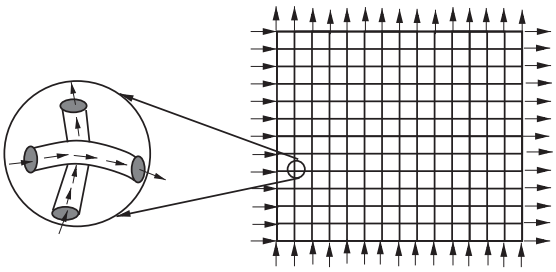

Fig. 4. Electricity ("pumped") controlled in the e_1 and e_2 directions on the boundary on the fiber network.

The following system parameters were used:

- external magnetic field: $B_1^{ext} = -1, B_2^{ext} = 1$ (Newton-second/Coulomb-meter),
- boundary values: $E_1 = E_o = 10^4,\ E_2 = E_o = 10^4$ (Newton/Coulomb),
- size of the sheet: 0.254 m $\times$ 0.254 (m) (=10 in $\times$ 10 (in)),
- nominal fiber radii = 0.0005 (m),
- lumped charged-masses: 50×50 (a 50×50 fiber network weave),
- area-based density of fabric = 0.15 (kilograms/meter^2), leading to lumped masses of $m_i = \frac{(0.254)^2 \times 0.15}{(50)^2}$ (kilograms),
- average Young's modulus of a fiber-segment $\mathbb{E} = 100$ (mega-Pascals) (a typical polymer), with a random statistical variation of ±10% from the mean governed by a Gaussian distribution,
- damping coefficient, $c = 0.01$ (N s/m),
- damage evolution parameter, $\lambda = 1$,
- trapezoidal time-stepping parameter $\phi = 0.5$ (mid-point rule),
- initial (upper limit) time-step size: $\Delta t = 0.000001$ (s),
- iterative tolerance per time step: TOL = 0.000001,
- iteration limit per time-step: $K_d = 6$.

Following common practice, for electromagnetic materials, we write $\epsilon = \epsilon^* \epsilon_r$ where $\epsilon^* = 8.854 \times 10^{-12}$ farads/m is the free space permittivity and ϵ_r is the relative permittivity or "dielectric" constant. The parameter choice for time $t = t_o$ was $\epsilon_r = 10$. The conductivity at time $t = t_o$ was set to $\sigma = 10^4$ Siemens/meter. Fig. 5 shows the progressive response of a fabric to current being pumped in the (initially) $\boldsymbol{e}_1$ and $\boldsymbol{e}_2$ directions on the boundary. The colors indicate the charge. Qualitatively, this response should be expected. In order to see this, consider that initially, assuming a zero velocity, the electromagnetic force acting on the fabric is

$$\begin{aligned}\boldsymbol{\Psi}^{em} &= \mathcal{P}E\boldsymbol{e}_1 + \sigma E\boldsymbol{e}_1 \times (B_1^{ext}\boldsymbol{e}_1 + B_2^{ext}\boldsymbol{e}_2) + \mathcal{P}E\boldsymbol{e}_2 + \sigma E\boldsymbol{e}_2 \\ &\quad \times (B_1^{ext}\boldsymbol{e}_1 + B_2^{ext}\boldsymbol{e}_2) \\ &= \mathcal{P}E(\boldsymbol{e}_1 + \boldsymbol{e}_2) + \sigma E(B_2^{ext} - B_1^{ext})\boldsymbol{e}_3. \end{aligned} \tag{7.1}$$

Initially, Gauss' law asserts that $\mathcal{P} = 0$, and thus

$$\boldsymbol{\Psi}^{em} = \sigma E(B_2^{ext} - B_1^{ext})\boldsymbol{e}_3. \tag{7.2}$$

In other words, the fabric will be initially pulled upwards, which is consistent with the numerical results. Thereafter, the charged state is non-zero, and there are deformation components in the $\boldsymbol{e}_1$ and $\boldsymbol{e}_2$ directions.

8. Extensions and conclusions

In general, the properties of most electrically-active materials are quite sensitive to the temperature. The interconversions of various forms of energy (electromagnetic, thermal, etc.) in a system are governed by the first law of thermodynamics,

$$\rho\dot{w} - \boldsymbol{T} : \nabla_x \dot{\boldsymbol{u}} + \nabla_x \cdot \boldsymbol{q} - \rho z = 0, \tag{8.1}$$

where w is the stored energy per unit mass (which is a function of the temperature, θ), θ is the temperature, ρ is the density, $\boldsymbol{T}$ is Cauchy stress, $\boldsymbol{u}$ is the displacement field, $\boldsymbol{q}$ is heat flux, and ρz is the rate of electromagnetic energy absorbed due to Joule heating

$$\rho z = a\boldsymbol{J} \cdot \boldsymbol{E}, \tag{8.2}$$

where $0 \leqslant a \leqslant 1$ is an absorption constant. A derivation of Joule-heating is given in Appendix C. If we consider (a) the effects of deformation and stress to be insignificant for heating and (b) the stored thermal energy per unit mass to be $w = C\theta$, we obtain

$$\rho C\dot{\theta} = a\boldsymbol{J} \cdot \boldsymbol{E} = a\sigma(\boldsymbol{E} + \boldsymbol{v} \times \boldsymbol{B}^{ext}) \cdot \boldsymbol{E}, \tag{8.3}$$

where C is the heat capacity per unit mass and $0 \leqslant a \leqslant 1$. The series of plots in Fig. 6 illustrates the average increase in temperature by post-processing according to (with $a = 0.1$)

$$\theta(t + \Delta t) = \theta(t) + \Delta t(\phi\mathcal{F}(t + \Delta t) + (1 - \phi)\mathcal{F}(t)), \tag{8.4}$$

where $\mathcal{F} = \frac{1}{\rho C}\left(a\sigma(\boldsymbol{E} + \boldsymbol{v} \times \boldsymbol{B}^{ext}) \cdot \boldsymbol{E}\right)$. For example, one can use the following decompositions (employing thermo-electromagnetic saturation conditions-Sigmoid functions):

- For the electrical permittivity:

$$\begin{aligned}\epsilon(\theta, \boldsymbol{E}) &= \epsilon_o(1 + \chi_E(\theta, \boldsymbol{E})) = \epsilon_o\epsilon_r(\theta, \boldsymbol{E}) \\ &= \epsilon_o\epsilon_r(\theta_R, \boldsymbol{E}_R)\mathcal{E}(\theta - \theta_R, \boldsymbol{E} - \boldsymbol{E}_R), \end{aligned} \tag{8.5}$$

where χ_E is the electric susceptibility, θ is the temperature and the last term is a representation around a reference state, for example, using saturation-type Sigmoid functions of the form

$$\begin{aligned}\mathcal{E}(\theta - \theta_R, \boldsymbol{E} - \boldsymbol{E}_R) &= 1 + \mathcal{K}_{E1}\left(1 + e^{-\gamma_{E1}(\theta - \theta_R)}\right)^{-1} \\ &\quad + \mathcal{K}_{E2}\left(1 + e^{-\gamma_{E2}||\boldsymbol{E} - \boldsymbol{E}_R||}\right)^{-1}, \end{aligned} \tag{8.6}$$

where the γ's and $\mathcal{K}$'s are material parameters, and the terms with subscript "R" are reference values.

- For the electrical conductivity:

$$\begin{aligned}\sigma(\theta, \boldsymbol{E}) = \sigma(\theta_R, \boldsymbol{E}_R)\Big(&1 + \mathcal{K}_{S1}(1 + e^{-\gamma_{S1}(\theta - \theta_R)})^{-1} \\ &+ \mathcal{K}_{S2}(1 + e^{-\gamma_{S2}||\boldsymbol{E} - \boldsymbol{E}_R||})^{-1}\Big). \end{aligned} \tag{8.7}$$

Generally speaking, for many materials, until a saturation threshold is met, $\epsilon_r(\theta, \boldsymbol{E})$ grows with θ and $\sigma(\theta)$ decreases with θ. See the treatise of Jackson [22] for reviews of the rich variety of possible dielectrical responses of materials, including atomistic-level discussions to motivate non-linear dielectric behavior. Thermal effects under further study, along with corresponding coupling to changes in electrical conductivity and permittivity, by the author.

In summary, this work investigated the deformation of electrified textiles in an externally supplied magnetic field. The electric field was delivered by running current through the fibers from an external power source. Since, as the fabric deforms, the current changes direction and magnitude. In order to simulate such a system, one must solve a set of coupled equations governing the charge distribution, current flow and system dynamics. The deformation of the fabric, as well as the charge distribution and current flow, are dictated by solving the coupled system of differential equations for the motion of lumped masses, which are related through the fiber-segments under the action of electromagnetically-induced forces acting on a reduced order network model, which was in turn coupled to reduced-order models for the electrodynamics. The effects of the electric and magnetic fields were investigated and quantitative numerical simulations were provided, using an approach based on a temporally-adaptive

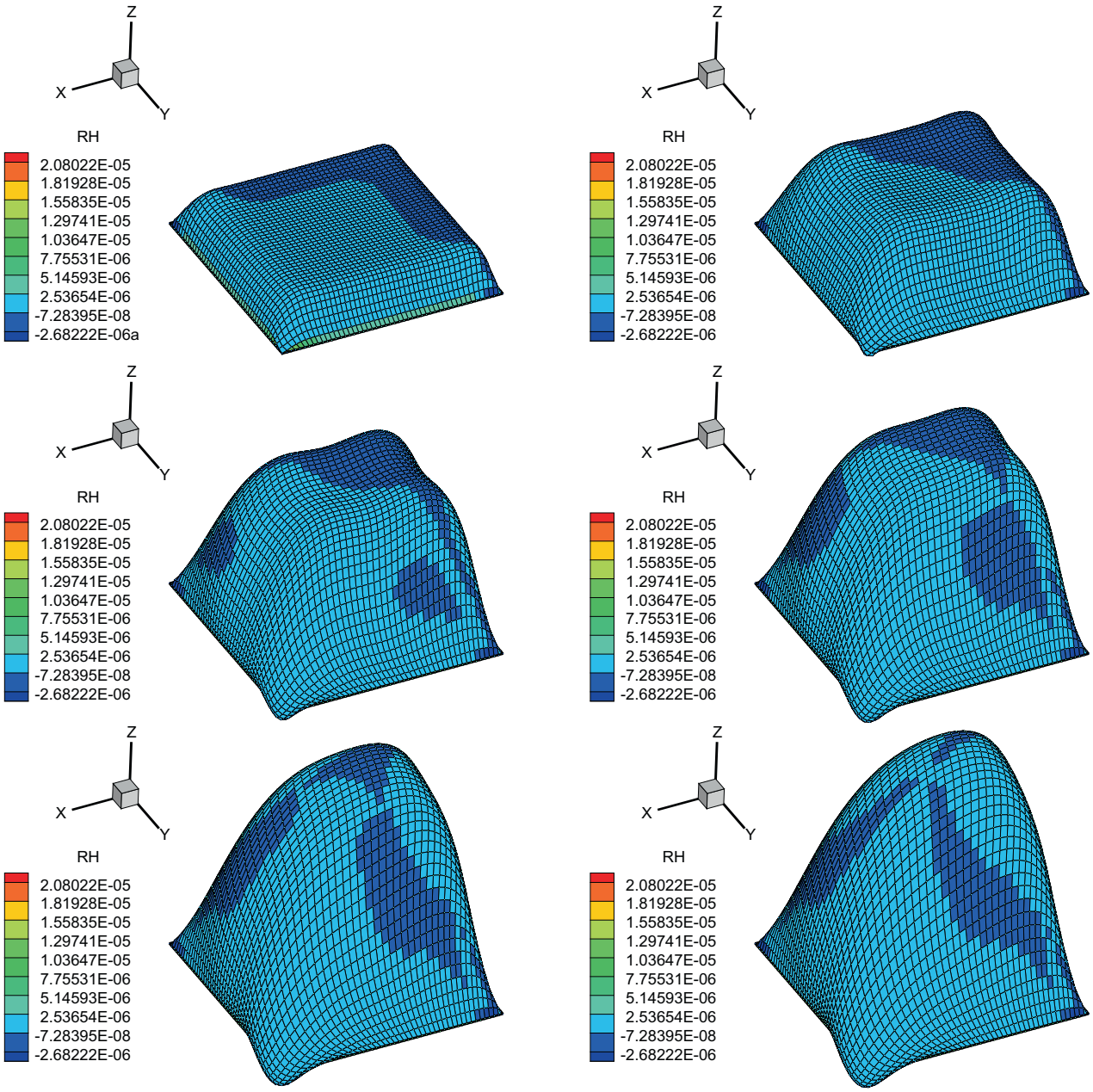

Fig. 5. Electricity pumped in the $\boldsymbol{e}_1$ and $\boldsymbol{e}_2$ directions from the boundary. The colors indicate the charge.

staggering time-stepping algorithm. A preliminary thermal analysis was provided and thermal effects are under current investigation by the author.

Acknowledgement

This work was funded in part by the Army Research Laboratory through the Army High Performance Computing Research Center (cooperative agreement W911NF-07-2-0027) and the Powley foundation.

Appendix A. Fabric materials

The base structural fabric materials that we are attempting to work with and modify are variants of Kevlar and Zylon, in conjunction with our university, industry and governmental partners (such as the Federal Aviation Administration (FAA), Boeing, Sandia National Laboratories and the Army Research Laboratories). We are attempting to modify these structural fabrics in order to endow them with enhanced conductivity for current carrying capabilities, while retaining these structural strength and light weight. *This experimental work is ongoing.* Generally, the microstructure of the fabric fibers is composed of several microscale fibrils. For example, fabric materials such as Zylon, which is a polymeric material produced by the Toyobo Corporation [45], Kevlar and other aramid-based materials have a microstructure comprised of bundles of microscale "microfibrils" forming the fibers, which is then tightly woven into sheets. For Zylon, each fiber contains approximately 350 microfibrils. In order to modify the mentioned structural fabrics, so that they have enhanced dielectric properties, while retaining these structural strength and light weight, two possible methods are

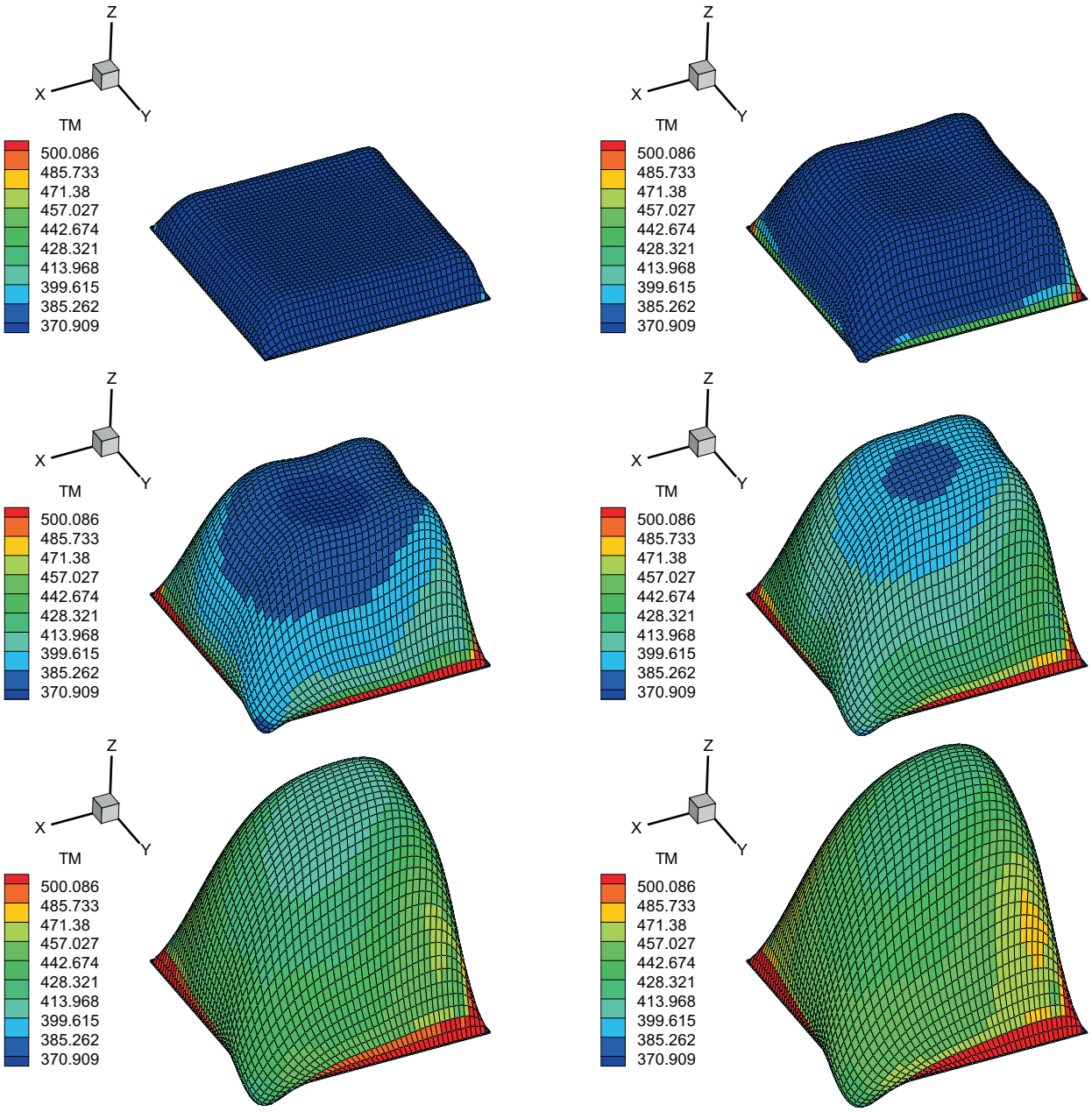

Fig. 6. Electricity pumped in the $\boldsymbol{e}_1$ and $\boldsymbol{e}_2$ directions. The colors indicate the temperature contribution from Joule-heating.

1. blending conducting dielectric material into the weave, such as mixtures of fine-scale iron powder and/or polydimethylsiloxane and
2. spraying/embedding the fabric with fine-scale conducting particles to produce desired overall effective conductivities.

The primary approach that we are following is (1). We are blending amounts of iron powder and polydimethylsiloxane into Kevlar and Zylon weaves. This type of material development is under investigation currently. We refer the reader to to recent published studies by Barham et al. [4–8] using/developing this type of material. We also note the existence of pure copper polyester Taffeta Fabric, which is a conductive material that we are also testing at UC Berkeley. We are also testing blends of Taffeta and Zylon and Taffeta and Kevlar. The computational tool developed in this paper is designed to help guide the material development and experimental work.

Remark: In order to illustrate the time-consuming complexity of experiments in this area, a few comments are in order on the testing processes for the base structural fabric materials. In particular, for a number of years we have focussed on on Zylon, which is a synthetic polymer produced by the Toyobo Corporation [45] constructed from woven PBO (Polybenzoxale) yarn. Over the last decade, experiments conducted at our laboratory at UC Berkeley have attempted to ascertain the number of sheets of Zylon needed to impede projectiles.[10] The typical amount of time taken for a single (labor intensive) ballistic test is rather lengthy, on the order of 90 min, and is described in detail in [27,47,52,57,37–39]. In order to perform the experiments, ballistic sheets of Zylon must be cut with a pair of special scissors from a fabric roll, clamped around a

[10] Reports, accessible to the public, can be obtained by making a request to the United States Federal Aviation Administration (FAA) indicating project 01-C-AW-WISU. For further experiments on individual yarn, see [46].

circular bar and placed into a square holder. The two parts of this square frame, whose outside dimensions are 356 mm with a 254 mm square window, are secured by 9.5 mm diameter hard steel bolts via an aluminum strip, which acts as a continuous washer. After these components are assembled, this device is clamped vertically to a heavy triangular support, which is mounted onto a 700 kg steel table so that impact is produced at a preselected location on the target, as specified by a laser beam mounted on the gun centerline. The tests are conducted using a custom built gas gun (12.9 mm inside diameter) with a 20 mm thick high strength steel barrel of 1.6 m length. This apparatus is mounted by means of a rail frame onto the same table as the target. The projectile usually consists of a 12.7 mm diameter steel cylinder with a mass of 36 g, with an aspect ratio of 3:1 which was heat treated to a Rockwell hardness of $R_c = 60$. Also, it is copper coated to a thickness of 0.5 mils to reduce barrel wear. A blast shield is placed in front of the muzzle to prevent interaction of ejected debris with the target. A projectile and fragment catcher, consisting of a large cloth filled container, is positioned beyond all final velocity measuring units. The tests are conducted inside an enclosed room which is evacuated during firing. The initial velocity of the projectile was determined from the time required to successively break two parallel laser beams, 156 mm apart, which were focused on two photodiodes, located 1.5 m in front of the target. The signals from the diodes initiate the start and stop modes of a Hewlett–Packard 5316 time interval meter. Final velocities are determined in three ways: (1) by the use of a digital video recording camera, operating at 10,000 frames/s, that capture the projectile position at a number of instances after the perforation using the dimensions of the projectile, (2) by means of two silver coated paper make-circuit grids spaced 50.4 mm apart, whose voltage pulses are directed to a time interval meter and (3) from two sets of 432×254 mm foils, with each pair separated by 12 mm and each set a distance of 12.7 mm apart, with the projectile contact providing an "on" circuit for each set, allowing the respective signals to start and stop a time interval meter. The number of desired sheets are cut and inserted in the target holder and the bolts were tightened with a 306 N-m torque wrench.

Appendix B. Time-scaling arguments for $\frac{\partial \mathcal{P}}{\partial t} \approx 0$

The formulation pumps electricity through the network, and accounts for any deformation changes the current through a balance law

$$\int_{\partial\Omega} \boldsymbol{J} \cdot \boldsymbol{n} dA + \int_{\Omega} \frac{\partial \mathcal{P}}{\partial t} dV = 0 \Rightarrow \nabla \cdot \boldsymbol{J} = 0, \tag{11.1}$$

where $\frac{\partial \mathcal{P}}{\partial t} = 0$ is assumed the current propagates through the fibers at a much faster time-scale than the deformation of the fabric. The velocity of the deformation of the fabric is far slower that the relative movement of charge (propagation of electricity) through the fabric (which is considered instantaneous). Changes in $\mathcal{P}$ are determined by the Gauss' law:

$$\int_{\partial\Omega} \boldsymbol{D} \cdot \boldsymbol{n} dA = \int_{\Omega} \mathcal{P} dV. \tag{11.2}$$

As an illustrative example, in order to appreciate the fast time scales that justify $\frac{\partial \mathcal{P}}{\partial t} \approx 0$, consider an arbitrary piece of continuum (undergoing no deformation) governed by

$$\nabla \cdot \boldsymbol{J} = \sigma \nabla \cdot \boldsymbol{E} = \frac{\sigma}{\epsilon} \nabla \cdot \boldsymbol{D} = \frac{\sigma}{\epsilon} \mathcal{P} = -\frac{\partial \mathcal{P}}{\partial t}, \tag{11.3}$$

where the following simple constitutive laws were used for illustration purposes: $\boldsymbol{J} = \sigma \boldsymbol{E}$, $\boldsymbol{D} = \epsilon \boldsymbol{E}$ and $\nabla \cdot \boldsymbol{D} = \mathcal{P}$. Solving for $\mathcal{P}$ yields

$$\mathcal{P}(\boldsymbol{x}, t) = \mathcal{P}(\boldsymbol{x}, t = 0) e^{-\frac{\sigma}{\epsilon} t}, \tag{11.4}$$

thus

$$\frac{\partial \mathcal{P}}{\partial t} = -\frac{\sigma}{\epsilon} e^{-\frac{\sigma}{\epsilon} t}. \tag{11.5}$$

The term $e^{-\frac{\sigma}{\epsilon} t}$ is extremely small since the ratio $\frac{\sigma}{\epsilon}$ is huge, for example, $\epsilon = 8.854 \times 10^{-12}$ Farads/meter and $\sigma = 10^4$ Siemens/meter, thus *leading to* $\frac{\sigma}{\epsilon} \approx 10^{15}$, and $-\frac{\sigma}{\epsilon} e^{-\frac{\sigma}{\epsilon} t} \approx 0$ for virtually any time-scales of interest, thus justifying $\int_{\partial\Omega} \boldsymbol{J} \cdot \boldsymbol{n} dA = 0$. In summary, any changes in $\mathcal{P}$ can be considered instantaneous, relative to mechanically-induced deformations.

Appendix C. Joule heating

Following a special case of general electromagnetic materials in [59], consider Faraday's Law

$$\nabla \times \boldsymbol{E} = -\frac{\partial \boldsymbol{B}}{\partial t} \tag{12.1}$$

and Ampere's Law

$$\nabla \times \boldsymbol{H} = \frac{\partial \boldsymbol{D}}{\partial t} + \boldsymbol{J} \tag{12.2}$$

where we recall that $\boldsymbol{E}$ is the electric field, $\boldsymbol{D}$ is the electric field flux, $\boldsymbol{J}$ is the electric current, $\boldsymbol{H}$ is the magnetic field and $\boldsymbol{B}$ is the magnetic field flux. Joule-heating can be motivated by forming the inner product of the magnetic field with Faraday's law and the inner product of the electric field with Ampere's law and forming the difference to yield

$$\underbrace{\boldsymbol{E} \cdot (\nabla \times \boldsymbol{H}) - \boldsymbol{H} \cdot (\nabla \times \boldsymbol{E})}_{-\nabla \cdot (\boldsymbol{E} \times \boldsymbol{H}) = -\nabla \cdot \boldsymbol{S}} = \boldsymbol{E} \cdot \boldsymbol{J} + \underbrace{\boldsymbol{E} \cdot \frac{\partial \boldsymbol{D}}{\partial t} + \boldsymbol{H} \cdot \frac{\partial \boldsymbol{B}}{\partial t}}_{= \frac{\partial W}{\partial t}}, \tag{12.3}$$

where $W = \frac{1}{2}(\boldsymbol{E} \cdot \boldsymbol{D} + \boldsymbol{H} \cdot \boldsymbol{B}) = \frac{1}{2}(\boldsymbol{E} \cdot \boldsymbol{\epsilon} \cdot \boldsymbol{E} + \boldsymbol{H} \cdot \boldsymbol{\mu} \cdot \boldsymbol{H})$ is the electromagnetic energy and where $\boldsymbol{S} = \boldsymbol{E} \times \boldsymbol{H}$ is the Poynting vector. Thus

$$\frac{\partial W}{\partial t} + \nabla \cdot \boldsymbol{S} = -\boldsymbol{J} \cdot \boldsymbol{E}. \tag{12.4}$$

Eq. (12.4) is usually referred to as Poynting's theorem, and can be interpreted, *for simple material laws, where the previous representation for W holds*, as stating that the rate of change of electromagnetic energy within a volume, plus the energy flowing out through a boundary, is equal to the negative of the total work done by the fields on the sources and conduction. We consider the absorbed energy that is available for heating to be proportional to the energy associated with conduction, namely, from Eq. (12.4), $\boldsymbol{J} \cdot \boldsymbol{E}$, and account for it via $\rho z = a \boldsymbol{J} \cdot \boldsymbol{E}$, where a is an absorption constant, $0 \leqslant a \leqslant 1$.

References

[1] A.A. Atai, D.J. Steigmann, On the nonlinear mechanics of discrete networks, Arch. Appl. Mech.. 67 (1997) 303–319.
[2] A.A. Atai, D.J. Steigmann, Coupled deformations of elastic curves and surfaces, Int. J. Solids Struct. 35 (16) (1998) 1915–1952.
[3] R.G. Azevedo, D.G. Jones, A.V. Jog, B. Jamshidi, D.R. Myers, L. Chen, X.A. Fu, M. Mehregany, M.B.J. Wijesundara, A.P. Pisano, A SiC MEMS resonant strain sensor for harsh environment applications, IEEE Sensors J. 7 (4) (2007) 568–576.
[4] M. Barham, D.J. Steigmann, M. McElfresh, R.E. Rudd, Finite deformation of a pressurized magnetoelastic membrane in a stationary dipole field, Acta Mech. 191 (2007) 1–19.
[5] M. Barham, D.J. Steigmann, M. McElfresh, R.E. Rudd, Limit-point instability of a magnetoelastic membrane in a stationary magnetic field, J. Smart Mater. Struct. 17 (2008) 6–11.
[6] M. Barham, D. White, D.J. Steigmann, R.E. Rudd, Finite-element modeling of the deformation of a thin magnetoelastic film compared to a membrane model, IEEE Trans. Magnet. 45 (2009) 4124–4127.
[7] M. Barham, D. White, D.J. Steigmann, Finite-element modeling of the deformation of magnetoelastic film, J. Comput. Phys. 229 (2010) 6193–6207.
[8] M. Barham, D.J. Steigmann, D. White, Magnetoelasticity of highly deformable thin films: Theory and simulation, Int. J. Nonlinear Mech. 47 (2012) 185–196.

[9] H.A. Buchholdt, M. Davies, M.J.L. Hussey, The analysis of cable nets, J. Inst. Maths. Appl. 4 (1968) 339–358.
[10] H. Bufler, B. Nguyen-Tuong, On the work theorems in nonlinear network theory, Ing. Arch. (1980) 49 275–286.
[11] M. Cannarozzi, A minimum principle for tractions in the elastostatics of cable networks, Int. J. Solids Struct. 23 (1987) 551–568.
[12] M. Cannarozzi, Stationary and extremum variational formulations for the elastostatics of cable networks, Meccanica 20 (1985) 136–143.
[13] Demkowicz, Computing with hp-Adaptive Finite Elements. I. One- and Two-Dimensional Elliptic and Maxwell Problems, CRC Press, Taylor and Francis, 2006.
[14] L. Demkowicz, J. Kurtz, D. Pardo, M. Paszynski, W. Rachowicz, A. Zdunek, Frontiers: Three Dimensional Elliptic and Maxwell Problems with Applications, Computing with Hp-Adaptive Finite Elements, vol. 2, CRC Press, Taylor and Francis, 2007.
[15] S. Ghosh, Micromechanical Analysis and Multi-Scale Modeling Using the Voronoi Cell Finite Element Method, CRC Press/Taylor & Francis, 2011.
[16] S. Ghosh, D. Dimiduk, Computational Methods for Microstructure-Property Relations, Springer, NY, 2011.
[17] C. Grimes, K. Ong, K. Loiselle, P. Stoyanov, D. Kouzoudis, Y. Liu, C. Tong, F. Tefiku, Magnetoelastic sensors for remote query environmental monitoring, Smart Mater. Struct. 8 (1999) 639–646.
[18] E.M. Haseganu, D.J. Steigmann, Analysis of partly wrinkled membranes by the method of dynamic relaxation, Comput. Mech. 14 (1994) 596–614.
[19] E.M. Haseganu, D.J. Steigmann, Theoretical flexural response of a pressurized cylindrical membrane, Int. J. Solids Struct. 31 (1994) 27–50.
[20] E.M. Haseganu, D.J. Steigmann, Equilibrium analysis of finitely deformed elastic networks, Comput. Mech. 17 (1996) 359–373.
[21] Z. Hashin, Analysis of composite materials: a survey, ASME J. Appl. Mech. 50 (1983) 481–505.
[22] J.D. Jackson, Classical Electrodynamics, third ed., Wiley, 1998.
[23] V.V. Jikov, S.M. Kozlov, O.A. Olenik, Homogenization of Differential Operators and Integral Functionals, Springer-Verlag, 1994.
[24] D.G. Jones, R.G. Azevedo, M.W. Chan, A.P. Pisano, M.B.J. Wijesundara, Low temperature ion beam sputter deposition of amorphous silicon carbide for vacuum encapsulation, in: Proceedings of the IEEE International Conference on Micro Electro Mechanical Systems, Kobe, Japan, 2007.
[25] D. Kouzoudis, C. Grimes, The frequency response of magnetoelastic sensors to stress and atmospheric pressure, Smart Mater. Struct. 9 (2000) 885–889.
[26] D. Kouzoudis, C. Grimes, Remote query fluid flow velocity measurement using magnetoelastic thick film sensors, J. Appl. Phys. 87 9 (2000) 6301–6303.
[27] K. Kwong, W. Goldsmith, Lightweight ballistic protection of flight-critical components on commercial aircraft – Ballistic characterization of zylon, FAA report DOT/FAA/AR-04/45, P1, 2004.
[28] P. Martin, Handbook of Deposition Technologies for Films and Coatings, third ed., Elsevier, 2009.
[29] P. Martin, Introduction to Surface Engineering and Functionally Engineered Materials, Scrivener and Elsevier, 2011.
[30] J.C. Maxwell, On the dynamical theory of gases, Philos. Trans. Soc. London. 157 (1867) 49.
[31] J.C. Maxwell, A treatise on electricity and magnetism, third ed., Ed, Clarendon Press, Oxford, 1873.
[32] D.R. Myers, K.B. Cheng, B. Jamshidi, R.G. Azevedo, D.G. Senesky, L. Chen, M. Mehregany, M.B.J. Wijesundara, A.P. Pisano, A silicon carbide resonant tuning fork for micro-sensing applications in high temperature and high G-shock environments, J. Micro/Nanolithography MEMS MOEMS 8 (2) (2009) 021116.
[33] S. Nemat-Nasser, M. Hori, Micromechanics: Overall Properties of Heterogeneous Solids, second ed., Elsevier, Amsterdam, 1999.
[34] P.D. Pangiotopoulos, A variational inequality approach to the inelastic stress-unilateral analysis of cable structures, Comput. Struct. 6 (1976) 133–139.
[35] M. Papadrakakis, A method for the automatic evaluation of the dynamic relaxation parameters, Comput. Methods Appl. Mech. Engrg. 25 (1980) 35–48.
[36] A.C. Pipkin, The relaxed energy density for isotropic elastic membranes, IMA J. Appl. Math. 36 (1986) 297–308.
[37] D. Powell, T.I. Zohdi, G. Johnson, Multiscale modeling of structural fabric undergoing impact, FAA report DOT/FAA/AR-08/38, 2008.
[38] D. Powell, T.I. Zohdi, Attachment mode performance of network-modeled ballistic fabric shielding, Compos. Part B: Engrg. 40 (6) (2009) 451–460.
[39] D. Powell, T.I. Zohdi, A note on flaw-induced integrity reduction of structural fabric, Int. J. Fract./Lett. Micromech. 158 (2009) L89–L96.
[40] J.W. Rayleigh, On the influence of obstacles arranged in rectangular order upon properties of a medium, Phil. Mag. 32 (1892) 481–491.
[41] E. Quandt, A. Ludwig, Magnetorestrictive actuation in microsystems, Sensors Actuators 81 (2000) 275–280.
[42] G.M. Rebeiz, N.S. Barker, J.B. Muldavin, G.-L. Tan, Mechanical Modeling of MEMS Devices: Static Analysis RF MEMS: Theory, Design and Technology, in: G.M. Rebeiz (Ed.), Wiley, New York, 2004, pp. 21–57.
[43] D.J. Steigmann, Tension field theory, Proc. Roy. Soc. London A 429 (1990) 141–173.
[44] S. Torquato, Random Heterogeneous Materials: Microstructure and Macroscopic Properties, Springer-Verlag, New York, 2001.
[45] Toyobo, PBO fiber ZYLON, Report of the Toyobo Corporation, LTD, 2001. <www.toyobo.co.jp>.
[46] J. Verzemnieks, Lightweight ballistic protection of flight-critical components on commercial aircraft – Zylon yarn tests, FAA report DOT/FAA/AR-05/45, P3, 2005.
[47] T.I. Zohdi, Modeling and simulation of progressive penetration of multilayered ballistic fabric shielding, Comput. Mech. 29 (2002) 61–67.
[48] T.I. Zohdi, D.J. Steigmann, The toughening effect of microscopic filament misalignment on macroscopic fabric response, Int. J. Fract. 115 (2002) L9–L14.
[49] T.I. Zohdi, Modeling and direct simulation of near-field granular flows, Int. J. Solids Struct. 42/2 (2004) 539–564.
[50] T.I. Zohdi, A computational framework for agglomeration in thermo-chemically reacting granular flows, Proc. Roy. Soc. 460 (2052) (2004) 3421–3445.
[51] T.I. Zohdi, Charge-induced clustering in multifield particulate flow, Int. J. Numer. Methods Engrg. 62 (7) (2005) 870–898.
[52] T.I. Zohdi, D. Powell, Multiscale construction and large-scale simulation of structural fabric undergoing ballistic impact, Comput. Methods Appl. Mech. Engrg. 195 (1-3) (2006) 94–109.
[53] T.I. Zohdi, Computation of strongly coupled multifield interaction in particle-fluid systems, Comput. Methods Appl. Mech. Engrg. 196 (2007) 3927–3950.
[54] T.I. Zohdi, A computational framework for network modeling of fibrous biological tissue deformation and rupture, Comput. Methods Appl. Mech. Engrg. 196 (2007) 2972–2980.
[55] T.I. Zohdi, Introduction to the Modeling and Simulation of Particulate Flows, SIAM Society for Industrial and Applied Mathematics, 2007.
[56] T.I. Zohdi, P. Wriggers, Introduction to Computational Micromechanics, Springer-Verlag, 2008 (Second Reprinting).
[57] T.I. Zohdi, Microfibril-based estimates of the ballistic limit of multilayered fabric shielding, Int. J. Fract./Lett. Micromech. 158 (2009) L81–L88.
[58] T.I. Zohdi, High-speed impact with electromagnetically sensitive fabric and induced projectile spin, Comput. Mech. 46 (2010) 399–415.
[59] T.I. Zohdi, Simulation of coupled microscale multiphysical-fields in particulate-doped dielectrics with staggered adaptive FDTD, Comput. Methods Appl. Mech. Engrg. 199 (2010) 79–101.
[60] T.I. Zohdi, Dynamics of clusters of charged particulates in electromagnetic fields, Int. J. Numer. Methods Engrg. 85 (2011) 1140–1159.
[61] T.I. Zohdi, Electromagnetically-induced deformation of functionalized fabric, J. Elast. 105 (1–2) (2011) 381–398.